VIII International Conference on Fracture Mechanics of Concrete and Concrete Structures
FraMCoS-8
J.G.M. Van Mier, G. Ruiz, C. Andrade, R.C. Yu and X.X. Zhang (Eds)

EVALUATION OF NONLOCAL APPROACHES FOR MODELLING FRACTURE IN NOTCHED CONCRETE SPECIMENS

DIMITRIOS XENOS*, PETER GRASSL* AND MILAN JIRÁSEK†

*University of Glasgow
School of Engineering, Glasgow, UK,
Rankine Building, University of Glasgow, G12 8QQ,
e-mails: d.xenos.1@research.gla.ac.uk, peter.grassl@glasgow.ac.uk

†Czech Technical University in Prague
Department of Mechanics, Faculty of Civil Engineering
Prague,Czech Republic
e-mail: Milan.Jirasek@fsv.cvut.cz

Key words: Concrete, Fracture mechanics, Nonlocal, Meso-scale, Lattice, Fracture process zone

Abstract. In concrete, growth and coalescence of microcracks lead to formation of visible fracture process zones that transfer stresses by crack bridging and aggregate interlock. Commonly, the behaviour of the fracture process zones is modelled by nonlinear fracture mechanics approaches using stress-strain laws with strain softening. One group of nonlinear fracture mechanics approaches suitable for computational structural analysis are nonlocal models, which lead to regular strain distributions over the fracture process zones, independently of the size of finite elements. This is achieved by evaluating the stress at each point based on weighted averages of state variables in the vicinity of that point. However, there is no consensus how the influence of boundaries should be taken into account by the averaging procedures. In the present comparative study, nonlocal damage models with different averaging methods and constitutive laws are investigated, with attention focused on the influence of boundaries. The most common approach of standard scaling is compared to averaging procedures that depend on the stress state and on the distance to boundaries. Firstly, the nonlocal models are calibrated by fitting stress-strain curves of one-dimensional uniaxial tension analyses to the results of mesoscale analyses. Then, the models are applied to two-dimensional simulations of three-point bending tests with a sharp notch, a 45° V-type notch and a smooth boundary without a notch. The performance of the nonlocal models is evaluated by comparison of load-displacement curves and dissipated energy profiles along the ligament of the beams with meso-scale results.

1 INTRODUCTION

The failure process of concrete strongly depends on the meso-structure. Growth and coalescence of microcracks lead to formation of visible fracture process zones transferring stresses by crack bridging and aggregate interlock. The response of these fracture process zones (FPZ) is commonly modelled by nonlinear fracture mechanics using stress-strain laws with softening. Within the group of computational methods, the various approaches proposed in the literature may be divided into two categories; namely meso-scale models describing explicitly the different phases of the heterogeneous material [4, 6], and macroscopic models based on an equivalent homogenized continuum [1].

In meso-scale models, it is convenient to de-

scribe the heterogeneity of the material by mapping the material properties of the individual phases on a background mesh [6]. The fracture process of the brackground mesh is often described as the progressive failure of discrete elements, such as beams or trusses [2,3]. In recent years, one discrete element method based on the Voronoi tessellation has been shown to be particularly suitable for modelling fracture [5]. The meso-scale approaches provide a detailed description of the crack patterns. However, a very fine discretisation and multiple analyses are required to obtain the averaged response.

Among macroscopic fracture approaches proposed in the literature, integral-type nonlocal models describe the fracture process zones as regions of highly concentrated but still regular strain [1,7]. Interactions at the mesoscale are reflected by weighted spatial averaging of internal variables. However, there is no consensus on how the averaging should be adjusted near the physical boundary of the body. Commonly used rescaling procedures may result in excessive spurious energy dissipation close to boundaries [9]. In alternative approaches, which have the potential to reduce this spurious effect, the averaging procedure depends on the distance to boundaries [10, 11] and on the stress state of the material point [12].

In the present work, three nonlocal damage models representing standard, distance-based and stress-based averaging procedures are applied to the modelling of fracture in notched concrete beams subjected to three-point bending. Initially, the models are calibrated by fitting meso-scale analysis results obtained for a problem independent of boundaries [4]. This calibration is thus unaffected by the type of averaging procedure used. Then, the nonlocal models are applied to simulations of two-dimensional notched beams subjected to three-point bending, for which the averaging procedure is expected to influence the response. The results of these analyses are again compared to the results of meso-scale analyses in the form of load-displacement curves and dissipated energy profiles.

2 MESO-SCALE MODEL

In this work, a meso-scale description of the fracture process in three-point bending tests has been used to create reference results for the evaluation of nonlocal models presented in Section 3. In this meso-scale approach, aggregates, interfacial transition zones (ITZ) and mortar are modelled as separate phases with different material properties. For the mortar and ITZ, a random field of tensile strength and fracture energy is applied. This meso-scale description has been performed by a lattice approach in combination with a damage mechanics model to describe the mechanical response of the three phases [5]. Since it had been used previously for the determination of fracture process zones of concrete subjected to uniaxial tension [4], it is here only briefly described.

2.1 LATTICE APPROACH

The nodes of the lattice are randomly located in the domain, subject to the constraint of a minimum distance, which is independent of the heterogeneity of the material. The lattice elements are obtained from the edges of the triangles of the Delaunay triangulation of the domain (solid lines in Fig. 1a), whereby the middle cross-sections of the lattice elements are the edges of the polygons of the dual Voronoi tessellation (dashed lines in Fig. 1a).

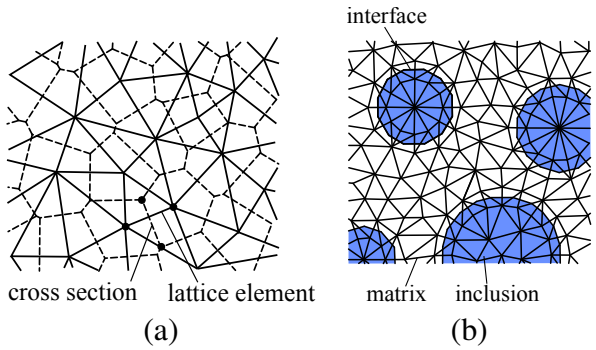

Figure 1: (a) Set of lattice elements (solid lines) with middle cross-sections (dashed lines) obtained from the Voronoi tessellation of the domain; (b) Arrangement of lattice elements around inclusions.

Each lattice node possesses three degrees of freedom, namely two translations and one ro-

tation. The degrees of freedom of the lattice nodes are linked to two displacement discontinuities at the centre of the middle cross-section of the element. The displacement discontinuities are transformed into strains by smearing them out over the distance between the two lattice nodes. The strains are related to the stresses by an isotropic damage model describing the constitutive response of ITZ and mortar.

The spatially varying material properties that originate from the heterogeneity of the material are reflected at two levels. Large aggregates are modelled directly by placing lattice nodes at special locations, such that the middle cross-sections of the lattice elements form the boundaries between aggregates and mortar (Fig. 1b). The heterogeneity represented by finer particles is described by autocorrelated random fields of tensile strength and fracture energy, which are assumed to be fully correlated. The random fields are characterised by an autocorrelation length that is independent of the spacing of lattice nodes. Discretely modelled aggregates are assumed to be linear elastic.

3 MACROSCOPIC MODEL

In this section, the macroscopic nonlocal isotropic damage mechanics approaches are described. The constitutive law and the different averaging procedures are described in Sections 3.1 and 3.2, respectively.

3.1 Damage model

The total stress-strain relationship for the isotropic damage model is

$$\boldsymbol{\sigma} \;=\; (1-\omega)\mathbf{D}_\mathrm{e} : \boldsymbol{\varepsilon} = (1-\omega)\tilde{\boldsymbol{\sigma}} \qquad (1)$$

where $\boldsymbol{\sigma}$ is the total stress tensor, ω is the damage variable, $\mathbf{D}_\mathrm{e}$ is the elastic stiffness based on Young's modulus E and Poisson's ratio ν, $\boldsymbol{\varepsilon}$ is the strain and $\tilde{\boldsymbol{\sigma}}$ is the effective stress tensor. Damage is driven by the history variable κ_d and is determined by

$$\omega\left(\kappa_\mathrm{d}\right) = \begin{cases} 1-\exp\left(-\frac{1}{m_\mathrm{d}}\left(\frac{\kappa_\mathrm{d}}{\varepsilon_\mathrm{max}}\right)^{m_\mathrm{d}}\right) & ,\kappa_\mathrm{d} \le \varepsilon_1 \\ 1-\frac{\varepsilon_3}{\kappa_\mathrm{d}}\exp\left(-\frac{\kappa_\mathrm{d}-\varepsilon_1}{\varepsilon_\mathrm{f}\left[1+\left(\frac{\kappa_\mathrm{d}-\varepsilon_1}{\varepsilon_2}\right)^n\right]}\right) & ,\kappa_\mathrm{d} > \varepsilon_1 \end{cases} \qquad (2)$$

where

$$m_\mathrm{d} \;=\; \frac{1}{\ln(E\varepsilon_\mathrm{max}/f_\mathrm{t})} \qquad (3)$$

The parameter ε_max is the uniaxial strain at peak stress. Furthermore,

$$\varepsilon_\mathrm{f} \;=\; \frac{\varepsilon_1}{(\varepsilon_1/\varepsilon_\mathrm{max})^{m_\mathrm{d}}-1} \qquad (4)$$

and

$$\varepsilon_3 \;=\; \varepsilon_1 \exp\left(-\frac{1}{m_\mathrm{d}}\left(\frac{\varepsilon_1}{\varepsilon_\mathrm{max}}\right)^{m_\mathrm{d}}\right) \qquad (5)$$

This damage law exhibits pre- and post-peak nonlinearities in uniaxial tension. The history variable κ_d, used in (2) to obtain the damage parameter, represents the maximum level of nonlocal equivalent strain $\bar{\varepsilon}_\mathrm{eq}$ reached in the history of the material. It is determined by the loading function

$$f\left(\bar{\varepsilon}_\mathrm{eq}, \kappa_\mathrm{d}\right) \;=\; \bar{\varepsilon}_\mathrm{eq} - \kappa_\mathrm{d} \qquad (6)$$

and by the loading-unloading conditions

$$f \le 0, \quad \dot{\kappa}_\mathrm{d} \ge 0, \quad \dot{\kappa}_\mathrm{d} f = 0 \qquad (7)$$

The nonlocal equivalent strain is defined as

$$\bar{\varepsilon}_\mathrm{eq}\left(\boldsymbol{x}\right) = \int_V \alpha\left(\boldsymbol{x},\boldsymbol{\xi}\right)\varepsilon_\mathrm{eq}(\boldsymbol{\xi})\mathrm{d}\boldsymbol{\xi} \qquad (8)$$

Here, $\boldsymbol{x}$ is the point at which the nonlocal equivalent strain $\bar{\varepsilon}_\mathrm{eq}$ is evaluated as a weighted average of local equivalent strains ε_eq at all points $\boldsymbol{\xi}$ in the vicinity of $\boldsymbol{x}$ within the integration domain V. According to the standard scaling approach, the weight function

$$\alpha\left(\boldsymbol{x},\boldsymbol{\xi}\right) = \frac{\alpha_0\left(\boldsymbol{x},\boldsymbol{\xi}\right)}{\int_V \alpha_0\left(\boldsymbol{x},\boldsymbol{\xi}\right)\mathrm{d}\boldsymbol{\xi}} \qquad (9)$$

is constructed from a function $\alpha_0(\boldsymbol{x},\boldsymbol{\xi})$ normalised by its integral over the integration domain V such that the averaging scheme does not modify a uniform field: The function

$$\alpha_0\left(\boldsymbol{x},\boldsymbol{\xi}\right) = \exp\left(-\frac{\|\boldsymbol{x}-\boldsymbol{\xi}\|}{R}\right) \qquad (10)$$

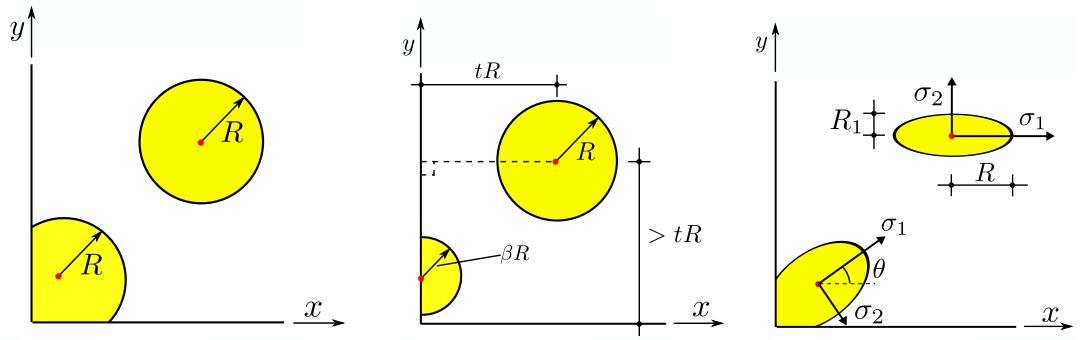

(a) (b) (c)

Figure 2: Three approaches to consider boundaries for nonlocal averaging: (a) standard, (b) distance-based and (c) stress-based rescaling.

is defined here as an exponential (Green-type) function, with parameter R reflecting the internal material length. The local equivalent strain in (8) is

$$\varepsilon_{\text{eq}} = \frac{1}{E} \max_{I=1,2,3} \tilde{\sigma}_I \tag{11}$$

where $\tilde{\sigma}_I$ refers to the principal components of the effective stress tensor introduced in (1). This constitutive law results in a Rankine strength envelope.

3.2 Approaches for treating boundaries

This section presents three different methods to treat boundaries. They are labelled as standard, distance-based and stress-based approach and represent groups of models presented in the literature (Fig. 2). Although the distance-based and stress-based averaging approaches are based on concepts previously reported in the literature, they have not been presented before in this form.

For the **standard rescaling approach**, the weight function $\alpha(\boldsymbol{x}, \boldsymbol{\xi})$ in (9) is used, with the integration domain V in the denominator of (9) corresponding to the specimen under consideration. Rescaling of the weight function according to (9) ensures that the nonlocal operator does not alter a uniform field.

For the **distance-based approach**, the weight function is also rescaled, but $\alpha_0(\boldsymbol{x}, \boldsymbol{\xi})$ in (10) is made dependent on the minimum distance of point $\boldsymbol{x}$ to the specimen boundary (Fig. 2b). The new function is

$$\alpha_0\left(\boldsymbol{x}, \boldsymbol{\xi}\right) = \exp\left(-\frac{\|\boldsymbol{x} - \boldsymbol{\xi}\|}{\gamma\left(\boldsymbol{x}\right) R}\right) \tag{12}$$

where

$$\gamma\left(\boldsymbol{x}\right) = \begin{cases} 1 & , d(\boldsymbol{x}) \geq tR \\ \dfrac{1-\beta}{tR} d(\boldsymbol{x}) + \beta & , d(\boldsymbol{x}) < tR \end{cases} \tag{13}$$

Here, β and t are parameters of the distance-based rescaling approach and $d(\boldsymbol{x})$ is the minimum distance of point $\boldsymbol{x}$ to the specimen boundary. For a material point $\boldsymbol{x}$ lying on the boundary ($d(\boldsymbol{x}) = 0$) the function yields $\gamma\left(\boldsymbol{x}\right) = \beta$. On the other hand, when the distance is greater than tR, $\gamma\left(\boldsymbol{x}\right) = 1$ and the present distance-based approach gives the same result as the standard rescaling approach.

The **stress-based rescaling approach** (Fig. 2c) exploits a transformation matrix

$$\mathbf{T} = \begin{pmatrix} \cos(\theta) & \sin(\theta) \\ -\sin(\theta)/\gamma & \cos(\theta)/\gamma \end{pmatrix} \tag{14}$$

which depends on the effective stress $\tilde{\boldsymbol{\sigma}}$. Angle $\theta = \operatorname{atan}\left(\mathrm{n}_{1\mathrm{y}}/\mathrm{n}_{1\mathrm{x}}\right)$ characterizes the direction of maximum principal effective stress $\tilde{\sigma}_1$, with n_{1y} and n_{1x} being the components of the corresponding eigenvector n_1. The new function

$$\alpha_0\left(\boldsymbol{x}, \boldsymbol{\xi}\right) = \exp\left(-\frac{\|\mathbf{T} \cdot (\boldsymbol{\xi} - \boldsymbol{x})\|}{R}\right) \tag{15}$$

is affected by the effective stress. In equation (14), γ is a scaling factor, defined as

$$\gamma = \begin{cases} \beta + (1-\beta)\left(\dfrac{\langle\tilde{\sigma}_2\rangle}{\tilde{\sigma}_1}\right)^2 & , \tilde{\sigma}_1 > 0 \\ 1 & , \tilde{\sigma}_1 \leq 0 \end{cases} \quad (16)$$

Here, β is a parameter of this approach, $\tilde{\sigma}_2$ is the second principal effective stress and $\langle\cdot\rangle$ denotes the MacAuley brackets (positive part operator). For instance, for uniaxial tension the principal effective stresses are $\tilde{\sigma}_1 = \tilde{\sigma}_\mathrm{t}$ and $\tilde{\sigma}_2 = 0$, which gives $\gamma = \beta$. On the other hand, for equi-biaxial tension we have $\tilde{\sigma}_1 = \tilde{\sigma}_2 = \tilde{\sigma}_\mathrm{t}$, so that $\gamma = 1$, which coincides with the standard rescaling approach.

4 ANALYSES

The nonlocal damage model combined with the different boundary approaches was applied to 2D plane-stress analyses of notched three-point bending tests. The geometry and the loading setup are shown in Fig. 3. Three boundaries in the form of a sharp notch with $\alpha = 0°$, an angular notch with $\alpha = 45°$ and an unnotched boundary with $\alpha = 90°$ were considered. The boundary types were chosen so that the performance of the boundary approaches (Section 3.2) could be compared.

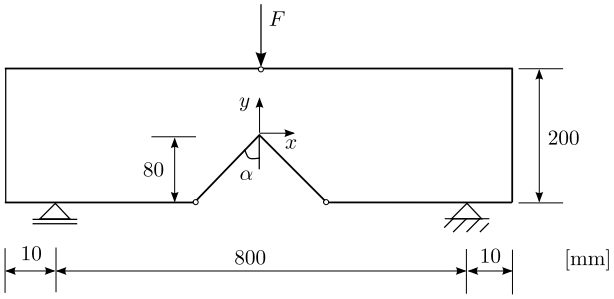

Figure 3: Geometry and loading setup of the notched beams subjected to three point bending.

Firstly, the parameters of the nonlocal model were calibrated, so that the model results for 1D tensile loading were in agreement with meso-scale results reported in [4]. For this calibration step, the results are not affected by the boundary approaches. This calibration resulted in elastic parameters of $E = 29.6$ GPa and $\nu = 0.2$. Furthermore, the parameters of the damage law are $f_\mathrm{t} = 2.86$ MPa, $\varepsilon_\mathrm{max} = 0.000198$, $\varepsilon_1 = 0.00023$ and $\varepsilon_2 = 0.007$. Finally, the nonlocal radius is $R = 0.004$ m. These parameters are the same as in [4]. The results of the calibration are shown in Fig. 4 in the form of stress-strain curves and dissipated energy across the fracure process zone. The stress-strain curve of the nonlocal model agrees well with the meso-scale results. The energy profile of the nonlocal model fits well the width of the FPZ obtained from meso-scale analyses but slightly underestimates the maximum energy dissipation in the middle of the specimen.

In the second step, the additional parameters of the distance-based model were chosen as $\beta = 0.35$ and $t = 1$ and for the stress-based model as $\beta = 0.35$. The results of the three nonlocal approaches for the three beam geometries are compared to meso-scale results in Figs. 5–7 in the form of load-displacement curves and dissipated energy profiles along the ligament length of the beam. As seen in parts (a) of the figures, the peak load of the meso-scale analysis is overestimated by the standard nonlocal model for all beam geometries. For $\alpha = 0°$ and 45°, this overestimation is accompanied by a much higher dissipation near the notch than in the meso-scale analyses; see Figs. 5b and 6b. The dissipated energy profiles for the stress-based and the distance-based are in much better agreement with the meso-scale results for these beam geometries. For $\alpha = 90°$ all models slightly overestimate the peak load. For the standard and stress-based aproach, the dissipated energy along the ligament is overestimated as well; see Fig. 7b. However, the energy peak near the notch, as observed for the $\alpha = 0°$ and 45° for the standard approach, is not present.

For both the distance and stress-based approach, the energy peaks close to the notch observed with the standard approach are removed, but the dissipated energy along the ligament is overestimated. Nevertheless, the stress-based approach requires only one parameter. Finally, the standard approach does not require any additional parameters, but suffers from excessive

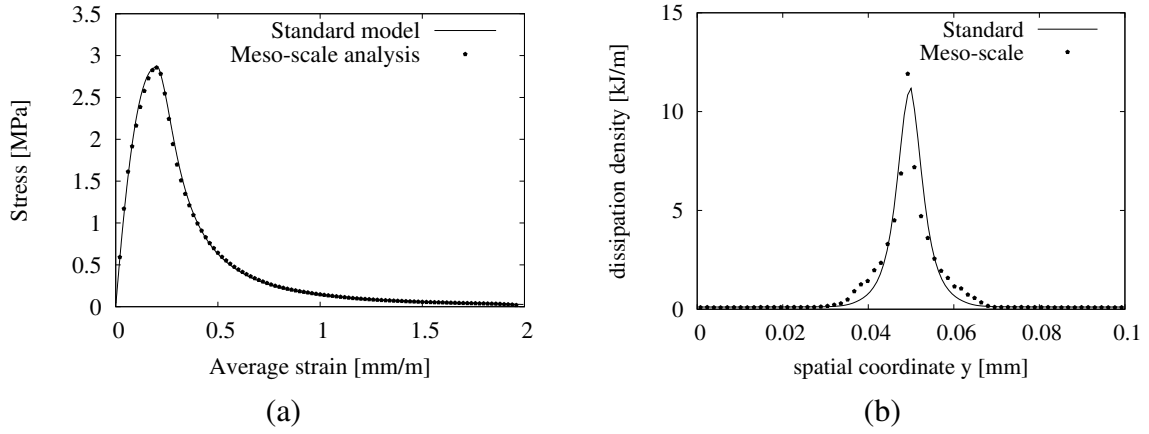

Figure 4: 1D calibration: (a) stress-strain curve, (b) Dissipated energy across the fracture process zone in the last loading step.

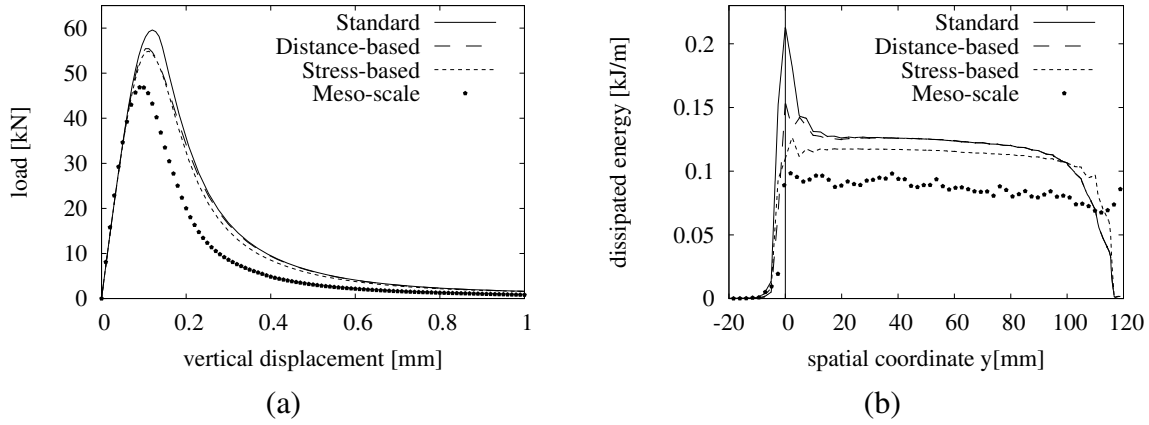

Figure 5: Comparison of the results of the three nonlocal approaches and meso-scale analysis for different notch angles $\alpha = 0°$: (a) Load-displacement curves and (b) Dissipated energy profiles.

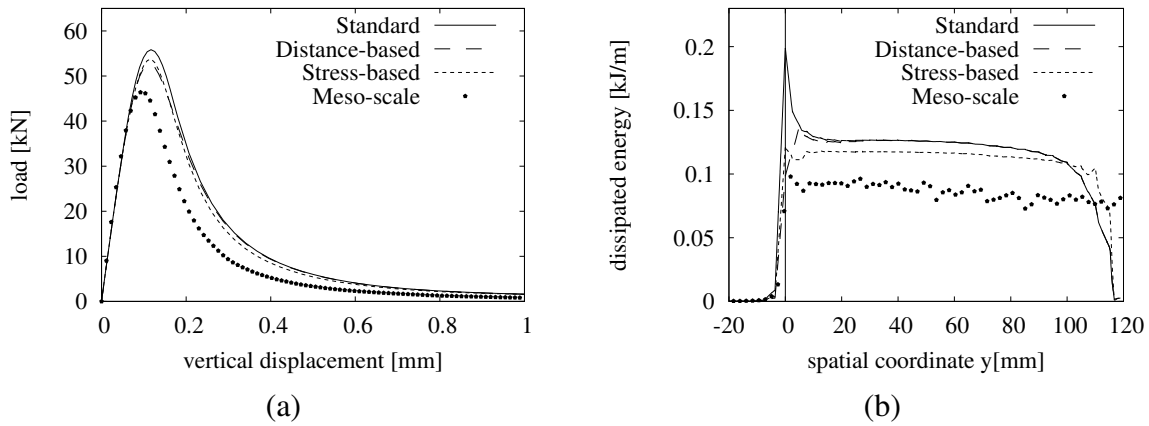

Figure 6: Comparison of the results of the three nonlocal approaches and meso-scale analysis for different notch angles $\alpha = 45°$: (a) Load-displacement curves and (b) Dissipated energy profiles.

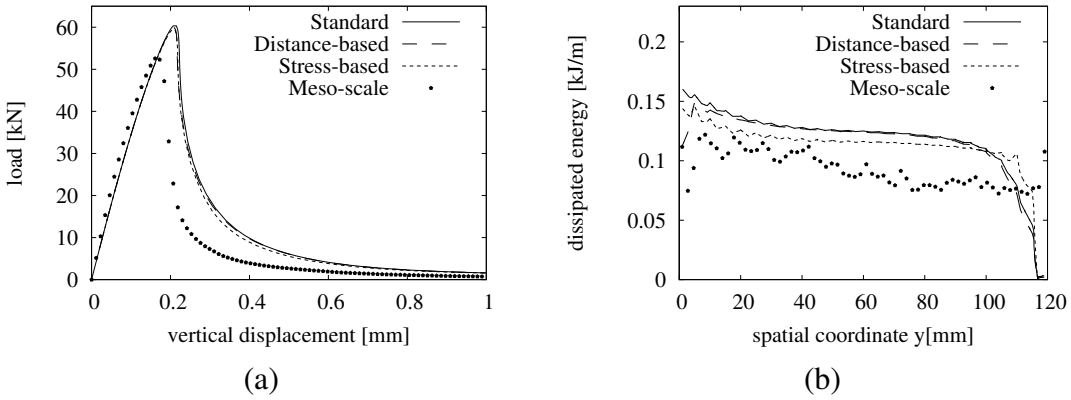

Figure 7: Comparison of the results of the three nonlocal approaches and meso-scale analysis for $\alpha = 90°$: (a) Load-displacement curves and (b) Dissipated energy profiles.

energy dissipation close to the notch.

The parameter β in both distance-based and stress-based methods influences the amount of nonlocal interactions in the weight function $\alpha(\boldsymbol{x}, \boldsymbol{\xi})$. A small value of β reduces the nonlocal contribution of the points $\boldsymbol{\xi}$ in the vicinity of the material point $\boldsymbol{x}$. If β is chosen too small, it results in a "local" definition of the nonlocal equivalent strain $\bar{\varepsilon}_{\text{eq}}$. Consequently, damage may localise in a single finite element or a single row of elements resulting in irregular strain profiles and mesh-dependent results. Therefore, a minimum value of $\beta = 0.35$ was enforced for the distance and stress-based approach so that the width of the localisation zone was larger than a row of finite elements. If a very fine mesh was used, β could be reduced further and it could be expected that the stress-based approach would yield an even better agreement with the meso-scale results.

5 CONCLUSIONS

In the present study, a nonlocal isotropic damage model with different averaging procedures was applied to the modelling of fracture in three-point bending test with different notch geometries. In the analyses of the sharp notched and V-notched beams, the standard approach overpredicts the energy dissipation close to the notch, which results in an overestimation of the load capacity. For the stress-based and distance-based averaging approaches, the energy dissipation close to the notch is reduced, which gives a better agreement with the meso-scale results. For the unnotched case, the dissipated energy is in reasonable agreement for all approaches. The distance-based approach requires two more input parameters than the standard approach, whereas the stress-based approach requires only one additional parameter over the standard approach.

In future work, the stress-based approach will be combined with a more advanced damage-plasticity model which can describe the failure of concrete in multiaxial stress states.

ACKNOWLEDGEMENT

The third author gratefully acknowledges financial support received from the Czech Science Foundation under project P105/10/2400.

REFERENCES

[1] Bažant, Z.P. and Jirásek, M., 2002. Nonlocal integral formulations of plasticity and damage: Survey of progress. *Journal of Engineering Mechanics* **128**:1119–1149.

[2] Kawai, T., 1978. New discrete models and their application to seismic response analysis of structures. *Nuclear Engineering and Design* **48**:207–229.

[3] Cundall, P.A and Strack, O. D. L., 1979. A discrete numerical model for granular assemblies. *Géotechnique* **29**:47–65.

[4] Grassl, P. and Jirásek, M., 2010. Meso-scale approach to modelling the fracture process zone of concrete subjected to uniaxial tension. *International Journal of Solids and Structures* **47**:957–968.

[5] Bolander, J.E. and Saito, S., 1998. Fracture analysis using spring networks with random geometry. *Engineering Fracture Mechanics* **61**:569–591.

[6] Schlangen, E. and van Mier, J. G. M., 1992. Simple lattice model for numerical simulation of fracture of concrete materials and structures. *Materials and Structures* **25**:534–542.

[7] Pijaudier-Cabot, G. and Bažant, Z.P., 1987. Nonlocal damage theory. *Journal of Engineering Mechanics* **113**:1512–1533.

[8] Jirásek, M. and Grassl., P., 2007. Boundary effect induced by nonlocal damage formulations. *CFRAC 2007; Proc of the International conference on computational fracture and failure of materials and structures*, Nantes, France, June 11-13, 2007.

[9] Jirásek, M., Rolshoven, S. and Grassl, P., 2004. Size effect on fracture energy induced by non-locality. *International Journal of Numerical and Analytical Methods in Geomechanics* **28**:653-670.

[10] Bolander, J. and Hikosaka, H., 1995. Simulation of fracture in cement-based composites. *Cement and Concrete Composites* **17**:135–145.

[11] Bažant, Z. P., Le, J.-L., and Hoover, C. G., 2010. Nonlocal boundary layer (NBL) model:Overcoming boundary condition problems in strength statistics and fracture analysis of quasibrittle materials. *Fracture Mechanics of Concrete and Concrete Structures/Recent Advances inFracture Mechanics of Concrete; Proc. of the 7th Inter. Conf. on Frac. Mech. of Conc. & Conc. Struct. (FraMCoS-7), 7*, May 23-28, 2010, Jeju, Korea pp. 135-143.

[12] Giry, C., Dufour, F., and Mazars, J., 2011. Stress-based nonlocal damage model. *International Journal of Solids and Structures* **48**:3431–3443.

[13] Grassl, P. and Jirásek, M., 2008. Meso-mechanically motivated nonlocal models for the modelling of the fracture process zone in quasi-brittle materials. *WCCM8; Proc. of the 8th World Congress on Computational Mechanics*, June 30-July 5, 2008, Venice, Italy.

[14] Patzák, B. and Bittnar, Z., 2001. Design of object oriented finite element code. *Advances in Engineering Software* **32**:759–767.

[15] Patzák, B., Rypl, D. and Bittnar, Z., 2001. Parallel explicit finite element dynamics with nonlocal constitutive models. *Computers and Structures* **79**:2287–2297.